

# Tunable photocycle kinetics of a hybrid bacteriorhodopsin/quantum dot system

Terianna J. Wax, Jordan A. Greco, Shutang Chen, Nicole L. Wagner, Jing Zhao (✉), and Robert R. Birge (✉)

55 North Eagleville Rd, Department of Chemistry, University of Connecticut, Storrs, CT, 06269-3060, USA

© Tsinghua University Press and Springer-Verlag GmbH Germany, part of Springer Nature 2018

Received: 3 August 2018 / Revised: 12 October 2018 / Accepted: 13 October 2018

## ABSTRACT

The inclusion of inorganic nanoparticles in biological environments has led to the creation of hybrid nanosystems that are employed in a variety of applications. One such system includes quantum dots (QDs) coupled with the photoactive protein, bacteriorhodopsin (BR), which has been explored in developing enhanced photovoltaic devices. In this work, we have discovered that the kinetics of the BR photocycle can be manipulated using CdSe/CdS (core/shell) QDs. The photocycle lifetime of protein samples with varying QD amounts were monitored using time-resolved absorption spectroscopy. Concentration-dependent elongations of the **bR** and **M** state lifetimes were observed in the kinetic traces, thus suggesting that excitonic coupling occurs between BR and QDs. We propose that the pairing of BR with QDs has the potential to be utilized in protein-based computing applications, specifically for real-time holographic processors, which depend on the temporal dynamics of the **bR** and **M** photointermediates.

## KEYWORDS

bacteriorhodopsin, photocycle, bionanotechnology, photochromism, quantum dot, hybrid materials

## 1 Introduction

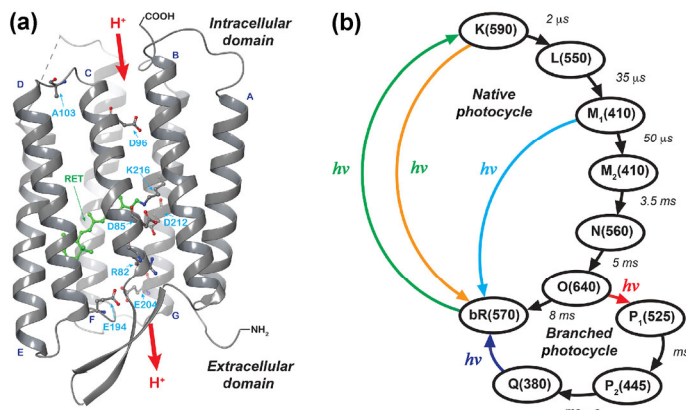
Advances in the development of bio-nanotechnologies have led to novel device constructs that interface the unique properties of biological and inorganic materials [1–3]. The success of such device architectures depends on the physical and chemical interactions between the biological materials and inorganic nanostructures [4–6]. One biomaterial that has been independently investigated for a number of bioelectronic applications is the protein, bacteriorhodopsin. Bacteriorhodopsin (BR) is a seven-transmembrane,  $\alpha$ -helical protein (Fig. 1(a)) that is expressed in the outer membrane of the *archaeon*, *Halobacterium salinarum* [7]. In *H. salinarum*, BR is arranged in trimers within a two-dimensional, semi-crystalline lattice known as the purple membrane (PM) [8, 9]. The chromophore of BR, all-*trans* retinal, is covalently bound to lysine-216 in helix G of the protein and is responsible for absorbing light close to the absorption maximum ( $\lambda_{\max}$ ) at 570 nm. The photoactivation of the protein initiates a well-characterized photocycle that results in the net translocation of a proton from the cytoplasmic surface to the extracellular domain of the membrane, which is coupled to energy production in the form of ATP under anaerobic conditions [10, 11]. Figure 1(a) highlights some of the key residues that are involved in the proton pumping pathway, in addition to alanine-103, which is the site of a critical point mutation that is the focus of this report.

Figure 1(b) features the native photocycle of bacteriorhodopsin, which describes the photochemically-activated isomerization event from all-*trans* to 13-*cis* retinal and the corresponding proton transfer pathway characterized by a series of spectrally distinct photointermediates. High quantum efficiencies have been recorded for the photochemical reaction that occurs to initiate the photocycle ( $\Phi \approx 0.65$ ) [12, 13]. The primary photoproduct of BR is often referred to as the **K** state ( $\lambda_{\max} = 590$  nm) and is characterized by a strained

13-*cis* chromophore conformation that drives all subsequent photocycle reactions [14–16]. Recent experimental and theoretical studies have also suggested the presence of sub-picosecond, transient photointermediates (the **I** and **J** states) that arise and decay in the ultrafast time regime before the **K** state and coincide with the *cis-trans* isomerization event [17–22]. Following the generation of **K**, the protein decays through a series of spectrally distinct photointermediates, including the **L**, **M**, **N**, and **O** states, before returning to the resting state (**bR**) [23]. Throughout the development of BR-based bio-nanotechnologies, the **M** state specifically has been of principal interest due to a hypsochromically-shifted  $\lambda_{\max}$  (410 nm) and amenable kinetic behavior (see below). Moreover, significant interest has been placed on the protein for application in non-native environments due to an inherently high thermal and photochemical stability once it is isolated in the PM from the native organism [7, 24, 25].

One of the most interesting photochemical properties of BR is the photochromic nature of the BR photocycle [26, 27]. As illustrated in Fig. 1(b), the photoactivation of BR is followed by the sequential decay of spectrally distinct photointermediates, however, if BR absorbs light with a wavelength of 410 nm during the lifetime of the **M** state, the **bR** resting state can be directly generated prior to the completion of the cycle [28]. This **M/bR** photochromic nature of BR has inspired the genesis of optically-based bioelectronic devices, including Fourier transform holographic associative processors. As opposed to serial memories that are used in modern computing architectures, associative processors are able to distinguish objects in real time and can implement the unique photochromic properties of BR to access and compare data blocks or images to others contained within the entire memory of the system. There has been interest in holographic computing systems due to the potential of simulating associative memory architectures akin to the human

Address correspondence to Jing Zhao, jing.zhao@uconn.edu; Robert R. Birge, rbirge@uconn.edu



**Figure 1** (a) Bacteriorhodopsin is native to the archaeon, *Halobacterium salinarum*, and has seven trans-membrane  $\alpha$ -helices with the chromophore, retinal (RET), covalently bound to lysine-216 (K216) in helix G. The A103C mutant is generated through site-directed mutagenesis at the intracellular side of the protein. (b) The main and branched photocycle of BR. The photointermediate lifetimes and absorption maxima (shown in parentheses and in units of nanometers) are included for each state.

brain [29, 30], thus suggesting significant applications in optically coupled neural network computers, robotic vision hardware, and other generic pattern recognition systems [31–34]. The design of our real-time holographic associative processors are based on work by Paek and Psaltis [33], and we continue to seek enhanced BR systems to optimize the *in situ* performance of the biomaterial in non-native environments (e.g., by using the presently described hybrid bio-inorganic systems).

In addition to the primary photocycle of BR, a branched photocycle exists that can be applied to long-term holographic processors [35]. Figure 1(b) demonstrates the branching reaction that is accessible following a sequential two-photon event, in which the native photocycle is first initiated and then the P/Q states are reached following red-light absorption during the lifetime of the O photointermediate. As opposed to the transient nature of the M state, the blue-shifted Q photoproduct ( $\lambda_{\max} = 380$  nm) can last up to several years at ambient temperature, leading to the application of the Q state for long-term memory storage. Additional work on the Q state in holographic architectures can be found in the literature, including efforts using genetic engineering and directed evolution to optimize the formation and stability of this unique photoproduct [36–39].

Quantum dots (QDs) are nanoscale semiconductors that are capable of harvesting a broad spectral range of light [40, 41]. Compared to organic fluorophores, QDs exhibit a number of advantageous properties for the inclusion in nano-biotechnologies, such as broad light absorption [42], narrow emission energies [40], and high photostability [41]. Moreover, the size tunability of colloidal QDs results in the emission of QDs over a large range of wavelengths across the electromagnetic spectrum due to the quantum confinement effect. Thus, QD nanoparticles have been incorporated into applications ranging from biodetection to solar cells [42, 43]. More recent efforts have focused on the coupling of QDs with biological materials, with a concentration on the photochemical interaction between QDs and BR [44–48].

As shown by Griep et al. [44], the pairing of CdSe/ZnS QDs with BR results in a nonradiative energy transfer between the QDs and BR that involves the Förster resonance energy transfer (FRET) mechanism. This energy transfer was found to be dependent on both the distance between the QDs and BR, and whether the QDs were coupled with either PM fragments or BR monomers. It was discovered that photoluminescence quenching of the QDs was more pronounced when the QDs were attached to the BR monomer

as a result of less steric hindrances and membrane folding which are prevalent in a PM fragment. An additional study focusing on the development of a bio-nanosensing device found that the energy coupling between QDs and BR-based thin films led to an enhancement in the photoelectric response of the protein [48]. Other studies have shown that the energy transfer via the FRET mechanism between QDs and the protein impacts the number of protons being pumped across the PM [46]. These studies have also illustrated how the inclusion of QDs with BR can broaden the spectral range of light absorption by BR beyond the 570 nm  $\lambda_{\max}$ . Furthermore, recent work has explored the effect of a magnetic field on CdSe QD photoluminescence, retinal isomerization, and the electron transfer process from an excited CdSe QD to an excited retinal chromophore [49]. Although there have been a multitude of studies proving the photoluminescence quenching of QDs by BR, there have been limited investigations that explore how QDs impact the kinetics of the BR photocycle.

In the present work, we demonstrate that the interaction between QDs and BR in solution allows for the direct modulation of the lifetime of the photocycle. CdSe/CdS QDs were added to individual solution samples of the BR mutant, A103C. This mutant was selected for this study to enable the conjugation between the PM fractions and QDs in solution. Select photointermediates were monitored via time-resolved absorption spectroscopy in the presence of QDs. As the relative concentration of QDs increased in solution, the **BR** and **M** decay lifetimes were incrementally elongated. Moreover, photoluminescence quenching of the QDs by BR was also evident from the QD fluorescence lifetime measurements indicative of a nonradiative energy transfer. From our experimental findings, we propose that excitonic coupling between BR and QDs leads to modified kinetics of the BR photocycle. The BR/QD hybrid system offers a new paradigm for creating BR-based holographic associative processors with tunable photochromic kinetics, which has previously not been achieved using traditional genetic or chemical modifications to the protein.

## 2 Experimental

### 2.1 Chemicals and buffers

All chemicals were either purchased from Thermo Fisher Scientific (Pittsburg, PA) or Sigma Aldrich (St. Louis, MO, USA), except for poly(ethylene glycol) methyl ether thiol (mPEG thiol, 500 MW), which was received from Rapp Polymere GmbH (Tübingen, Germany).

### 2.2 Strain generation, protein isolation, and purification

In order to generate the A103C BR mutant, mutant DNA was transformed into the MPK409 cell line of *H. salinarum* using methods outlined by Peck et al. [50]. Purple membrane fractions were then prepared and isolated according to standard procedures [51].

### 2.3 Synthesis and aqueous phase transfer of CdSe/CdS quantum dots

CdSe/CdS (core/shell) QDs were synthesized following established protocols [52, 53]. In order to render the CdSe/CdS QDs water soluble, a ligand exchange procedure was implemented [53]. First, 10 mg of poly(ethylene glycol) methyl ether thiol (mPEG thiol) was dissolved in 5 mL of chloroform in a 25 mL flask. 2 mL of the CdSe/CdS QDs solution (2.5 mg/mL) was added dropwise to the solution while stirring. The flask was covered with tin foil, degassed with nitrogen for 5 min, and allowed to stir overnight. The QDs were purified by adding ethanol and centrifuging at 11,000 rpm for 20 min to remove excess surfactants. The final products were redispersed in distilled water, and the absorption and emission spectra

of the sample were taken with a Cary-60 (Agilent) UV-visible spectrophotometer and a Fluoromax spectrofluorometer (Horiba Scientific), respectively. These spectra can be found in Fig. S1 in the Electronic Supplementary Material (ESM). A low resolution transmission electron microscopy (TEM) image of the QDs was obtained with a JEOL JEM-2010 microscope that had an accelerating voltage of 200 kV. Based on the TEM image, the diameter of the QDs was estimated to be  $8.9 \pm 0.7$  nm. The TEM image is shown as Fig. S2 in the ESM.

## 2.4 Preparation and characterization of the hybrid A103C/QD samples

Hybrid A103C/QD constructs were prepared by adding varying amounts of a QD stock solution (76.2 nM) to A103C samples with a concentration of 76.0  $\mu$ M (Fig. S3 in the ESM). The A103C aliquots in each mixture were held constant at 1.98 mg/mL ( $7.60 \times 10^{-9}$  moles), while the QD quantity was increased and the buffer volume was adjusted to maintain a consistent final volume as shown in Table S1 in the ESM.

The A103C/QD molar ratios calculated for each solution sample were the following: 900:1, 700:1, 500:1, 300:1, and 100:1. Molar ratios were adjusted based on the molarities and added volumes of QD and A103C stock solutions. Relatively low concentrations of QDs were used in this study to reduce sample aggregation and investigate whether minimal disturbances would alter the photochemical behavior of the protein. All hybrid samples were prepared in a 50 mM glycine buffer at pH 9.5. Each sample was mixed for 2 h at room temperature using a nutating mixer and was then centrifuged twice at 7,500 rpm for 30 min to remove unattached QDs in the supernatant. Finally, the samples were resuspended in a 50 mM glycine buffer at pH 9.5.

The absorption and emission spectra for the samples were taken with a Cary-60 (Agilent) UV-visible spectrophotometer and a Fluoromax spectrofluorometer (Horiba Scientific), respectively (Fig. S4 in the ESM). Although optimal spectral overlap is needed to achieve the greatest energy coupling between the BR absorption and QD emission, a QD emission spectrum ( $\sim 622$  nm) red-shifted with respect to the BR absorption maximum ( $\lambda_{\max} = 570$  nm) was chosen for this investigation. As shown in Fig. 5, the red-shifted QD emission promotes energy transfer between the **BR** and primary photointermediate states (i.e., **K** state) and limits the QD emission influence on later photointermediates, such as the **M** state. A detailed discussion on the impact of this red-shifted QD emission on the BR photointermediates can be found in the proposed mechanism.

## 2.5 Time-resolved photoluminescence measurements

Each sample was photoexcited with a supercontinuum pulsed laser (Solea, PicoQuant,  $\sim 100$ – $120$  ps pulse duration, 2.5 MHz repetition rate) that was tuned to a 532 nm excitation wavelength, and the photoluminescence of the samples was focused onto a single-photon detector ( $\tau$ -SPAD, PicoQuant) equipped with a suitable spectral filter. The photoluminescence lifetimes were obtained with a time-dependent single photon counting module (PicoHarp 300, PicoQuant) with a time resolution set at 32 ps. The photoluminescence decays were then fitted to a biexponential function (Table S2 in the ESM) to determine the lifetime values. All experiments were performed under ambient conditions.

## 2.6 Time-resolved absorption spectroscopy

Each protein sample was prepared at an optical density of 1.0 at the 570 nm  $\lambda_{\max}$  and transferred to 1.5 mL methacrylate cuvettes (Plastibrand Cuvettes, Fisher Scientific, Inc.) that have a 1-cm path length. Prior to the time-resolved measurements, the protein samples were light adapted (LA) using 400 W white light source for one hour.

A Neodymium:YAG laser system (Continuum Minilite II) was used as the actinic pump pulse directly preceding the time-resolved absorption measurements. The photocycle was initiated by photoexciting each sample using a 532 nm pulsed laser. A rapid-scanning monochromator (RSM) system (OLIS Instruments Inc., RSM-1000 stopped flow) was used to collect the time-resolved difference absorption spectra from 350 to 750 nm (via 50 L/mm, 500 nm blaze wavelength gratings) at a 1 ms time resolution with respect to the BR resting state absorption spectrum. The initial absorption spectrum of LA BR was used as a baseline and the RSM system monitored the difference spectra by using 1,000 scans averaged per second. The time-resolved difference spectra showed the formation and decay of the **BR** and **M** photointermediates (Fig. S5 in the ESM). The data gathered from these difference spectra were then used to generate heat maps that also illustrate the evolution of the photocycle and are shown here in this report (Fig. 3). In addition to gathering the time-resolved difference spectra for selected photointermediates, single-wavelength kinetic measurements for the **M** state following light activation were measured by averaging 10 traces per protein sample using a flash-photolysis set-up. In this set of experiments, the transmitted beam was set to 532 nm and passed through a monochromator, which was fixed at 410 nm. Single-wavelength kinetic traces for the **M** state (Fig. 4) were obtained by tracking changes in absorption at 410 nm using a photomultiplier tube. Equation (1) is used for the multiexponential fitting of the kinetic data, as implemented in the Birge software program, FitDynamics 3.2.2U

$$y(t) = A_0(1 - e^{-(t-t_0)/\tau_{\text{form}}}) - (e^{-(t-t_0)/\tau_{\text{decay}}}) \quad (1)$$

where  $A_0$  is the absorption at the time of laser excitation,  $t_0$  is the excitation time,  $\tau_{\text{form}}$  is the time constant for formation of the state, and  $\tau_{\text{decay}}$  is the time constant for the decay of the state. A schematic of the time-resolved apparatus can be found in Scheme S1 in the ESM. All the data were collected at 25  $^{\circ}$ C.

## 3 Results and discussion

### 3.1 Assembly of the A103C/QD hybrid system

The primary structure of *wild-type* BR contains no indigenous cysteine residues, however, previous reports have employed  $X \rightarrow C$  substitutions in order to offer a means to chemically examine structural/functional attributes of the protein using thiol-mediated spin label probes [54–56]. When the targeted mutation is located in the interhelical loop regions of BR (e.g., Q3C, S35C, A103C, M163C), cysteine-to-gold thiol linkages can be formed to anchor oriented monolayers of the protein for use in photoelectric device applications [57, 58]. The semicrystalline lattice of BR trimers in the PM fragments ensures that this binding is effectively irreversible, which is an attractive feature for generating stable BR thin films on a metal interface. This methodology has been enhanced in recent years by Watts et al. by isolating BR mutant trimers from the PM suspension and improving the surface molecular density of BR when applied onto gold films [59]. The BR/QD hybrid system created in this study does not utilize delipidated protein, although the methods do offer an opportunity to further improve upon the molecular interactions within the hybrid systems under development.

The mutant protein used in this study, A103C, has a history of use in efficient immobilization that exhibits *wild-type* structural and functional integrity [55, 60]. Because the mutation is located in the cytoplasmic loop region of the protein, the amino acid substitution does not have a significant impact on the proton translocation events comprised within the BR photocycle. Thus, this mutant has found application in studies that wish to anchor the protein while relegating the structural change to be photochemically inert.

In this report, the mPEG thiol surfactant coating the CdSe/CdS QDs was chosen to promote the solubility of the QDs in an aqueous solution and to facilitate bioconjugation to the A103C protein material. Based on the structure of this polymer, the thiol linkages will statistically bind to the CdS shell, thus burying many of the moieties for direct linkage to the cysteine residue in the A103C protein. However, as the spectroscopic analysis below indicates, there is evidence of a concentration-dependent A103C/QD interaction, which suggests the possibility of aberrant thiol groups that are exposed resulting in nonspecific binding of the QDs to the protein. Moreover, the electrostatic interactions between QDs and the PM have been previously demonstrated and offer an additional means of stabilizing the hybrid materials used in this study [45, 49].

Figure 2 shows the time-dependent photoluminescence decay of the A103C/QD conjugates collected at room temperature with varying A103C to QD ratios. The fluorescence lifetime is shown to decrease as the molar ratio of A103C to QDs is increased. Hence, samples that had higher concentrations of A103C relative to QD concentration (i.e., 900:1, A103C:QD) had more fluorescence quenching of the QDs compared to samples that had lower A103C concentrations, resulting in shorter fluorescence lifetimes. The photoluminescence lifetimes were calculated using a biexponential fit and the time constants  $\tau_1$  and  $\tau_2$  were found to decrease from 13.4 to 1.9 ns and 34.2 to 15.1 ns, respectively, trending toward higher A103C/QD molar ratios.

Table 1 shows the lifetime values obtained after fitting the photoluminescence decays for each sample. Additional fitting parameters can be found in Table S2 in the ESM. The observed phenomenon, which is also found in the emission spectra of the A103C/QD assemblies (Fig. S4(a) in the ESM) suggests a nonradiative energy transfer from the QDs to the protein ( $\lambda_{\max} = 570$  nm), that mirrors observations of FRET-like energy transfer in previous BR/QD investigations [44, 47–49, 61, 62].

One such study conducted by Griep et al. [44] demonstrated how the photoluminescence lifetimes were similarly measured to decrease upon the addition of BR to a QD solution ( $\tau = 13.3$  ns) relative to

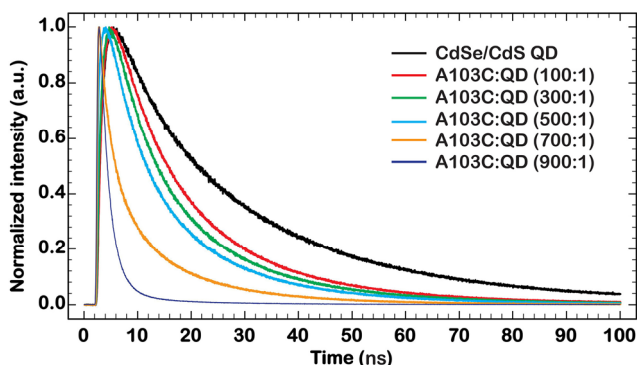


**Figure 2** QD photoluminescence lifetimes when colloidal QDs are assembled onto A103C. The photoluminescence lifetimes are indicative of a nonradiative energy transfer that occurs between the QDs and A103C in solution. At higher A103C/QD molar ratios, a decrease in the QD photoluminescence lifetime was observed.

**Table 1** Photoluminescence lifetimes for A103C/QD samples

Sample	$\tau_1$ (ns)	$\tau_2$ (ns)
QD	13.4 ± 0.07	34.2 ± 0.1
100:1	10.6 ± 0.07	22.9 ± 0.2
300:1	9.3 ± 0.04	23.2 ± 0.2
500:1	7.6 ± 0.04	20.1 ± 0.1
700:1	2.6 ± 0.01	13.7 ± 0.02
900:1	1.9 ± 0.004	15.1 ± 0.4

the untreated QD sample ( $\tau = 18$  ns). As noted above, this data does not necessarily confirm the extent of covalent linkages formed between the cysteine residue and the mPEG thiol surfactants, however, the fluorescence behavior signifies a close association between the two species in solution and is indicative of an energy transfer from the QD to retinal chromophore.

### 3.2 Time-resolved absorption spectroscopy

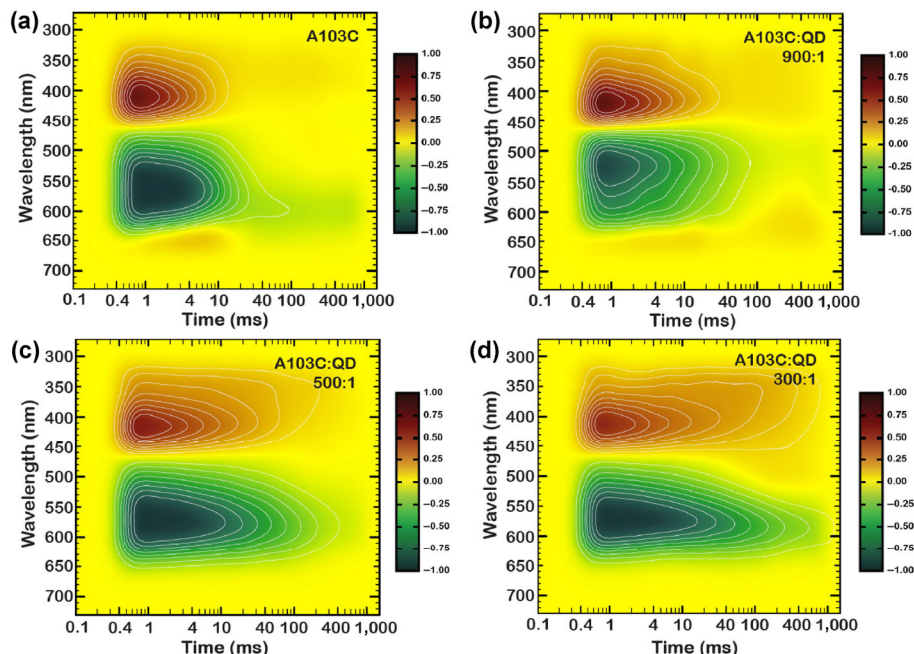
Upon confirmation of fluorescence quenching as a result of QD conjugation to A103C, the photocycle kinetics of A103C were monitored utilizing time-resolved absorption spectroscopy. The time-resolved absorption difference spectra were collected from zero to one second following irradiation at 532 nm (Fig. S5 in the ESM). The millisecond time resolution of this technique is capable of monitoring specific photointermediates of the BR photocycle, including the **bR** (570 nm), **M** (410 nm), and **O** (640 nm) states (Fig. 1(b)). While previous studies have investigated the impact of QDs on broadening the excitation energy range of BR and enhancing photocurrent generation [45, 46, 48, 63], this series of experiments investigates the consequences on the kinetics of the photocycle.

Figure 3 provides heat maps to track the time-dependent evolution of key photointermediates for varying relative concentrations of A103C and QD in aqueous solution (50 mM glycine, pH 9.5). As the concentration of QDs rise relative to the protein in the assemblies, the overall lifetime of the photocycle is shown to increase significantly. This result is clearly seen in the two-dimensional heat maps in Fig. 3, in which the positive and negative peaks at 410 nm (**M**) and 570 nm (**bR**), respectively, lengthen with increasing QD content. The **bR** state photokinetic lifetimes were collected based on the  $\lambda_{\max}$  values defined by the time-resolved difference spectra and range from 15.0 ms (A103C) to 68.8 ms (300:1, A103C:QD). Although chemical modifications to the protein that elongate the photocycle have been demonstrated previously [64–66], the QD concentration dependence of the **bR** and **M** state lifetimes we discovered here establishes a technique in creating a photochromic material with tunable dynamics (see below).

For all the samples shown in Fig. 3, there is little to no **O** state present in the plotted heat maps. This phenomenon is likely due to the experimental conditions that were used for the measurements (50 mM glycine, pH 9.5), which facilitated the deprotonation of the thiol groups for assembling the protein to the QDs. At pH 9.5, the photocycle is truncated to omit the **O** state because of the slow reprotonation of the deprotonated proton release complex [67, 68]. Concomitant with the disappearance of the **O** photointermediate at alkaline pH values is a truncation of the **M** state [69], which is offset in this study by the photochemical coupling with the CdSe/CdS QDs. Below, we discuss the implications of directly modulating the **M** state lifetime, particularly in reference to the application of these hybrid systems as photochromic media for Fourier transform holographic associative processors [24, 70, 71].

### 3.3 Tunable M state kinetics for photochromic applications

To determine the approximate rise and decay kinetics of the **M** photointermediate, each curve was fit to a double exponential (Eq. (1)). Figure 4 shows the kinetic traces at 410 nm for each A103C/QD sample. With increasing QD concentrations in the hybrid conjugated systems, the **M** state lifetime values ( $\tau_{\text{form}} + \tau_{\text{decay}}$ ) were shown to rise from 6.5 ms (A103C control) to 17.5 ms, 37.2, 48.2, and 62.7 ms (900:1, 700:1, 500:1, 300:1, respectively). Interestingly, the decreased rate of **M** state kinetics we observed is the opposite of what has been previously reported for BR/QD hybrid systems [72, 73]. This finding will be discussed in greater detail in the proposed mechanism section below. The importance of the **bR** (570 nm) → **M** (410 nm) photochemical reaction is derived from the spectral separation and change in refractive index of the transient **M**



**Figure 3** Two-dimensional heat maps for (a) A103C, (b) 900:1, (c) 500:1, and (d) 300:1 were created to monitor the evolution of the **M** and **bR** photointermediates. Both the 100:1 and 700:1 data sets are not included due to noise. As represented on the heat maps, elongations in the **M** (410 nm, positive red peak) and **bR** (570 nm, negative green peak) states are observed for A103C/QD solutions that contain higher QD concentrations (Panels (c) and (d)).

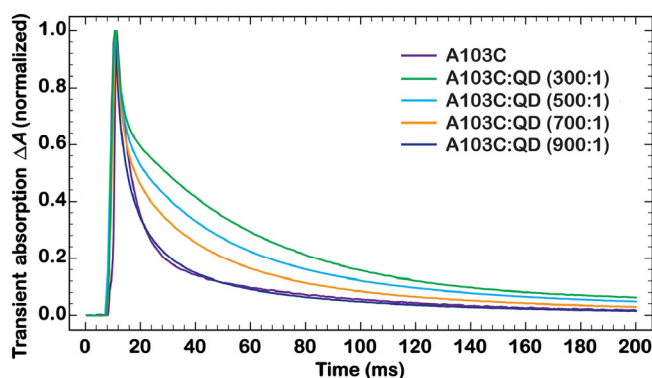


**Figure 4** **M** state kinetic traces gathered for each A103C/QD sample. A concentration dependence of QDs on the **M** state decay kinetics was observed, and the kinetic traces were fitted with a double exponential fitting equation to determine the **M** state lifetimes.

photointermediate with respect to the **bR** resting state. The photochemically reversible **bR/M** photochromic pair has led to the development of real-time holographic associative processors and next-generation bioelectronic devices.

However, because the **M** state lifetime is on the order of  $\sim 8$  ms (Fig. 1(b)), this metastable photointermediate of *wild-type* BR is fundamentally too short for the direct application into associative memory processors that rely on this photochemistry. Thus, the ability to alter the observed lifetime of the **M** state has been the subject of many research efforts since the first holographic associative processor was developed in the 1980s [74, 75].

Past studies have demonstrated the elongation of the BR photocycle by means of low-temperature trapping [28], dehydration [76], and various chemical modifications [64–66]. However, there is limited flexibility in the dynamics of these processes and the implementation of the environments are typically incongruous with the long-term stability of the biomaterial in devices. Chemical modifications using retinal analogues, particularly 4-keto retinal, have also been shown to introduce a dramatic increase in the **M** state lifetime [77, 78]. Finally, genetic engineering offers a robust framework for

modulating the photophysical properties and kinetics of the **bR/M** photochromic pair [79–81]. The most notable example is D96N, which has been shown to increase the **M** state lifetime to  $\sim 200$  ms at pH 5 and  $\sim 20$  s at pH 8 [31]. Nonetheless, the photochemical kinetics remain to be finite beyond the intentional disruption of the proton translocation pathway.

The results from this study demonstrate the direct manipulation of the photocycle lifetime by varying the amount of CdSe/CdS QDs relative to protein concentration. The use of A103C allows for close association of BR with the QD nanoparticles, and future efforts will continue to optimize the conjugation between the biological and inorganic materials. While further studies are necessary to understand the limitations and long-term stability of the excitonic coupling that is observed within the A103C/QD hybrid system, the results here present an interesting medium for incrementally modifying the dynamics of BR. In the concluding section of this report, we postulate the potential photochemical and physical mechanisms that are regulating these experimental observations.

### 3.4 Excitonic coupling in the A103C/QD hybrid system

Based on our experimental findings, we propose that excitonic coupling between the retinal chromophore of BR and QDs is the primary mechanism that is responsible for the observed alteration of the BR photocycle. The pairing of delocalized excited states has a significant effect on not only the electronic structure of the system, but also on the optical properties and energy transfer kinetics. Nonradiative energy transfer between the excited QDs and excited retinal is well established in Refs. [44, 47–49, 61, 62]. As shown previously [49], the spin-dependent photoluminescence quenching of QD nanoparticles by adsorbed BR leads to an efficient nonradiative energy transfer that requires the excitation of both retinal and the QDs. This cooperative mechanism is facilitated in our experiments through the 532 nm actinic pulse, which can lead to the simultaneous absorption of both materials within the system. Additionally, the A103C/QD hybrid assembly has shown to dramatically increase the nonlinear refractive index compared to BR solutions, thus suggesting a highly interacting system that may be regulated by excitonic coupling of the inorganic and biological materials [45]. Notably, the

enhancement of the nonlinear optical properties of BR is advantageous for the proposed application of the hybrid material within Fourier transform holographic thin films [24, 82].

Since the lifetime of the excited retinal occurs on a femtosecond timescale and the excited QD exciton can exist on the order of nanoseconds, we propose that the electron density of the retinal chromophore prior to isomerization undergoes a competitive event originating from the nonradiative energy transfer from the QDs, which obstructs isomerization during the ultrafast regime of the putative *I/J* states and distorts the subsequent procession of proton translocation events. This behavior was demonstrated by Roy et al. [49], in which quenching by the excited retinal molecule impacts the initiation and progression of the photocycle. The timescale of the excitonic coupling between the two materials is so fast, that it is unlikely that there is energy directly transferred from the QDs to retinal throughout the later photointermediates of the BR photocycle (i.e., the *M* state). Moreover, the 622 nm emission maximum of the QDs has very little spectral overlap with the blue-shifted *M* photointermediate ( $\lambda_{\text{max}} = 410$  nm) (Fig. 5). However, the primary photochemical event leading to the retinal isomerization occurs within several femtoseconds and the decay lifetime of the *K* photointermediate is on the order of  $\sim 2$   $\mu\text{s}$  [63]. Hence, the energy coupling that exists between the QDs and retinal can lead to perturbations in the *K* photointermediate lifetime. In addition to the fast timescale of this excitonic coupling, spectral overlap of the QD photoluminescence is greatest with that of the *bR* ( $\lambda_{\text{max}} = 570$  nm) and *K* ( $\lambda_{\text{max}} = 590$  nm) states as shown in Fig. 5. Thus, nonradiative energy transfer is optimal during the primary photocycle events, which can have consequences on the free-energy-driven progression of the photocycle following the formation of the *K* state [83]. This interference with the *K* state can, in turn, alter BR photodynamics/proton pumping and lead to downstream kinetic consequences, including the formation and decay of the blue-shifted *M* state.

In contrast to the observed consequences of A103C/QD excitonic coupling in this report, previous studies have indicated that the mixture of these biological and inorganic materials led to an increased rate of *M* state formation and decay (from  $\sim 5$  ms for PM complexes to  $\sim 3$  ms for PM/QD hybrid systems) [72, 73]. These reports suggested that the surface potential of the PM was altered due to the field effects of the negatively charged QDs, thus impacting the deprotonation and protonation kinetics of the protein. Similarly, El-Sayed et al. [63, 84, 85] have demonstrated an increased rate of decay of the *M* state in the presence of the plasmonic field of gold nanoparticles. While the CdSe/CdS QDs used in this investigation are not identical to those

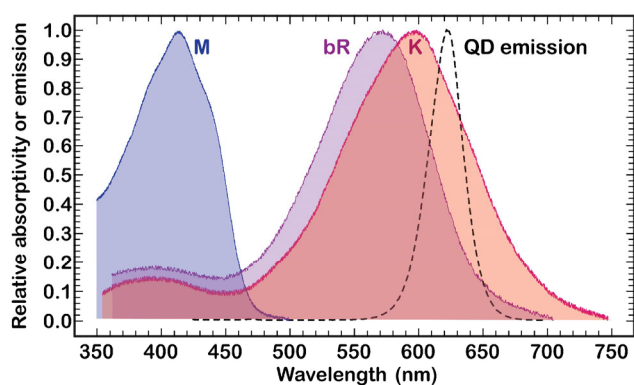


**Figure 5** The normalized photoluminescence spectrum of CdSe/CdS QDs at 622 nm, and the normalized absorption maxima of the *M* (410 nm), *bR* (570 nm), and *K* (590 nm) photointermediates. We propose that, due to the greater spectral overlap of the QD emission with that of the *bR* and *K* state absorption maxima, nonradiative energy transfer is likely during the primary photochemical events of the BR photocycle. (The *K* state spectrum is reproduced with permission from Ref. [24], © American Chemical Society 1999).

observed heretofore, it is interesting that we observed the opposite behavior of previous BR hybrid systems shown in the literature.

Discrepancies in the *M* state decay kinetics between our findings and others could stem from the synthetic design of our hybrid system, which would impact the BR/QD coupling. Although we did not employ direct binding methods, QD adsorption onto the PM surfaces was possible due to the potential of exposed thiol groups on the QD surfaces. Adhesion of the QDs onto the PMs could influence a variety of factors that would affect the retinal isomerization and ultimately photocycle kinetics. Concomitant with nonradiative energy transfer in our hybrid system, localized changes in the pH of the BR environment upon addition of QDs may lead to the observed perturbations in the photointermediate lifetimes [86]. Furthermore, the mPEG thiol coating around the QDs results in a slightly negatively charged QD surface that can electrostatically interact with the PMs [46, 47, 62, 87, 88]. As previously demonstrated in the literature, the negatively charged QDs could create an external electric field around the charged PM surface, hence leading to a modified PM surface potential and modulations in photocycle kinetics [74, 89, 90]. In addition to FRET-like energy transfer between the QDs and A103C, we do not rule out the potential of charge transfer impacting the QD photoluminescence lifetimes and *M* state kinetics. As shown in Refs. [49, 53, 91, 92], charge transfer is probable when there is optimal band energy alignment between the QDs and that of the HOMO and LUMO of retinal. While we did not directly measure the valence and conduction band energies of the QDs and the energies of the HOMO and LUMO of retinal, we infer that charge transfer is an additional mechanism that can influence the photocycle kinetics and further work is being undertaken to investigate this alternative pathway in our hybrid system.

The excitonic coupling model that is proposed above must be probed further to fully delineate the mechanism, however, it is likely that there is a mixture of chemical and physical phenomena that are contributing to our photochemical kinetic measurements above. We do not rule out the potential impact that mechanical fixation of the QDs may have on the dynamics of the proton pumping activity of BR. The PEG-capped QDs are known to have larger hydrodynamic diameters ( $\sim 10$  nm) than QDs capped with smaller ligands, such as cysteine [47]. Hence, increasing the concentration of these larger sized QDs may have the potential for limiting the conformational flexibility of BR in solution and potentially providing a barrier for efficient proton uptake or release. Nonetheless, the concentration dependence of the observed photochemical dynamics across multiple QD-BR-assembly paradigms, including the electrostatic adsorption of QDs encapsulated with a positively charged polymer onto *wild-type* BR (Fig. S6 in the ESM), suggests that photochemical coupling plays a more significant role. Similar to the A103C/QD series, elongations in the *M* and *bR* photointermediate lifetimes were observed for solutions of *wild-type* BR and positively charged QDs. In future studies, we will continue to investigate our mutant and *wild-type* hybrid systems as photochromic materials in holographic associative processor prototypes. Furthermore, femtosecond scale transient absorption spectroscopy will be used to investigate the *K* photointermediate to better understand the mechanism of the hybrid system.

## 4 Conclusions

Modulation of the BR photocycle is demonstrated by adjusting the concentration of CdSe/CdS QDs relative to the BR mutant, A103C, in solution. Specifically, this report measures the concentration-dependent, time-resolved absorption dynamics of the protein within a QD hybrid system, in which a mutant is used to directly attach the QD nanoparticle to the PM. We observe an increase in the lifetime of the photocycle in addition to the tunable modulation of

the blue-shifted **M** photointermediate. The ability to deliberately modulate the photochemical kinetics of the **BR/M** photochromic pair offers an approach in generating a medium that is adjustable for application in holographic associative processors and other applications that rely on specific photochemical dynamics of BR. We hope that this report inspires future investigations that continue to develop new device architectures that exploit the interface of biological and inorganic materials.

## Acknowledgements

Work in the laboratory of R. R. B. was supported by grants from the National Institutes of Health (GM-34548) and the Harold S. Schwenk Sr. Distinguished Chair in Chemistry. Work in the laboratory of J. Z. was partially supported by the National Science Foundation (No. CAREER-1554800). We also thank Nathan B. Gillespie for the **K** state spectrum shown in Fig. 5 of this report. (The **K** state spectrum is reproduced with permission from Ref. [24], © American Chemical Society 1999).

**Electronic Supplementary Material:** Supplementary material ((1) a table listing the volumes and number of moles of A103C, QD, and buffer used for the A103C/QD assemblies, (2) a table listing the fitting parameters for the A103C/QD fluorescence ensemble lifetime measurements, (3) a scheme illustrating the experimental setup of the time-resolved absorption spectrometer apparatus used to monitor the photocycle kinetics, (4) a figure showing the emission and absorbance spectra of CdSe/CdS (core/shell) QDs, (5) TEM image of the CdSe/CdS QDs, (6) images of the A103C/QD samples under visible and ultraviolet light, (7) a figure showing the emission and absorbance spectra of the A103C/QD solutions, (8) a figure showing the time-resolved difference spectra of the A103C/QD assemblies, (9) a figure showing the time-resolved heat maps of the hybrid constructs of the WT-BR/QD series, and (10) references) is available in the online version of this article at <https://doi.org/10.1007/s12274-018-2224-4>.

## References

- [1] Parpura, V. Bionanoelectronics: Getting close to the action. *Nat. Nanotechnol.* **2012**, *7*, 143–145.
- [2] Noy, A. Bionanoelectronics. *Adv. Mater.* **2011**, *23*, 807–820.
- [3] Maine, E.; Thomas, V. J.; Bliemel, M.; Murira, A.; Utterback, J. The emergence of the nanobiotechnology industry. *Nat. Nanotechnol.* **2014**, *9*, 2–5.
- [4] Nel, A. E.; Mädler, L.; Velegol, D.; Xia, T.; Hoek, E. M. V.; Somasundaran, P.; Klaessig, F.; Castranova, V.; Thompson, M. Understanding biophysicochemical interactions at the nano–bio interface. *Nat. Mater.* **2009**, *8*, 543–557.
- [5] Verma, A.; Stellacci, F. Effect of surface properties on nanoparticle–cell interactions. *Small* **2010**, *6*, 12–21.
- [6] Alkilany, A. M.; Lohse, S. E.; Murphy, C. J. The gold standard: Gold nanoparticle libraries to understand the nano–bio interface. *Acc. Chem. Res.* **2013**, *46*, 650–661.
- [7] Oesterhelt, D.; Stoekenius, W. Rhodopsin-like protein from the purple membrane of *Halobacterium halobium*. *Nat. New Biol.* **1971**, *233*, 149–152.
- [8] Luecke, H.; Schobert, B.; Richter, H. T.; Cartailler, J. P.; Lanyi, J. K. Structure of bacteriorhodopsin at 1.55 Å resolution. *J. Mol. Biol.* **1999**, *291*, 899–911.
- [9] Henderson, R.; Baldwin, J. M.; Ceska, T. A.; Zemlin, F.; Beckmann, E.; Downing, K. H. Model for the structure of bacteriorhodopsin based on high-resolution electron cryo-microscopy. *J. Mol. Biol.* **1990**, *213*, 899–929.
- [10] Stuart, J. A.; Birge, R. R. Characterization of the primary photochemical events in bacteriorhodopsin and rhodopsin. In *Biomembranes*. Lee, A. G., Ed.; JAI Press: London, 1996; pp 33–139.
- [11] Lozier, R. H.; Niederberger, W.; Bogomolni, R. A.; Hwang, S.; Stoekenius, W. Kinetics and stoichiometry of light-induced proton release and uptake from purple membrane fragments, *Halobacterium halobium* cell envelopes, and phospholipid vesicles containing oriented purple membrane. *Biochim.*

- Biophys. Acta* **1976**, *440*, 545–556.
- [12] Oesterhelt, D.; Hegemann, P.; Tittor, J. The photocycle of the chloride pump halorhodopsin. II. Quantum yields and a kinetic model. *EMBO J.* **1985**, *4*, 2351–2356.
- [13] Govindjee, R.; Balashov, S. P.; Ebrey, T. G. Quantum efficiency of the photochemical cycle of bacteriorhodopsin. *Biophys. J.* **1990**, *58*, 597–608.
- [14] Lanyi, J. K. Bacteriorhodopsin. *Annu. Rev. Physiol.* **2004**, *66*, 665–688.
- [15] Hayashi, S.; Tajkhorshid, E.; Schulten, K. Structural changes during the formation of early intermediates in the bacteriorhodopsin photocycle. *Biophys. J.* **2002**, *83*, 1281–1297.
- [16] Edman, K.; Nollert, P.; Royant, A.; Beirhali, H.; Pebay-Peyroula, E.; Hajdu, J.; Neutze, R.; Landau, E. M. High-resolution X-ray structure of an early intermediate in the bacteriorhodopsin photocycle. *Nature* **1999**, *401*, 822–826.
- [17] Schenk, S.; van Mourik, F.; van der Zwan, G.; Haacke, S.; Chergui, M. Probing the ultrafast charge translocation of photoexcited retinal in bacteriorhodopsin. *Science* **2005**, *309*, 917–920.
- [18] Kobayashi, T.; Salto, T.; Ohtani, H. Real-time spectroscopy of transition states in bacteriorhodopsin during retinal isomerization. *Nature* **2001**, *414*, 531–534.
- [19] Herbst, J.; Heyne, K.; Diller, R. Femtosecond infrared spectroscopy of bacteriorhodopsin chromophore isomerization. *Science* **2002**, *297*, 822–825.
- [20] Atkinson, G. H.; Brach, T. L.; Blanchard, D.; Rumbles, G. Picosecond time-resolved resonance Raman spectroscopy of the initial trans to cis isomerization in the bacteriorhodopsin photocycle. *Chem. Phys.* **1989**, *131*, 1–15.
- [21] Nogly, P.; Weinert, T.; James, D. Carbajo, S.; Ozerov, D.; Furrer, A.; Gashi, D.; Borin, V.; Skopintsev, P.; Jaeger, K. et al. Retinal isomerization in bacteriorhodopsin captured by a femtosecond X-ray laser. *Science*, in press, DOI: 10.1126/science.aat0094.
- [22] Nango, E.; Royant, A.; Kubo, M.; Nakane, T.; Wickstrand, C.; Kimura, T.; Tanaka, T.; Tono, K.; Song, C. Y.; Tanaka, R. et al. A three-dimensional movie of structural changes in bacteriorhodopsin. *Science* **2016**, *354*, 1552–1557.
- [23] Balashov, S. P. Protonation reactions and their coupling in bacteriorhodopsin. *Biochim. Biophys. Acta* **2000**, *1460*, 75–94.
- [24] Birge, R. R.; Gillespie, N. B.; Izaguirre, E. W.; Kusnetzow, A.; Lawrence, A. F.; Singh, D.; Song, Q. W.; Schmidt, E.; Stuart, J. A.; Seetharaman, S. et al. Biomolecular electronics: Protein-based associative processors and volumetric memories. *J. Phys. Chem. B* **1999**, *103*, 10746–10766.
- [25] He, J. A.; Samuelson, L.; Li, L.; Kumar, J.; Tripathy, S. K. Bacteriorhodopsin thin-film assemblies—Immobilization, properties, and applications. *Adv. Mater.* **1999**, *11*, 435–446.
- [26] Stuart, J. A.; Marcy, D. L.; Birge, R. R. Photonic and optoelectronic applications of bacteriorhodopsin. In *Bioelectronic Applications of Photochromic Pigments*. Dér, A.; Keszthelyi, L., Eds.; IOS Press: Szeged, Hungary, 2000; pp 16–29.
- [27] Tallent, J.; Song, Q. W.; Li, Z. F.; Stuart, J.; Birge, R. R. Effective photochromic nonlinearity of dried blue-membrane bacteriorhodopsin films. *Opt. Lett.* **1996**, *21*, 1339–1341.
- [28] Hampp, N. Bacteriorhodopsin as a photochromic retinal protein for optical memories. *Chem. Rev.* **2000**, *100*, 1755–1776.
- [29] Cutsuridis, V.; Wennekers, T. Hippocampus, microcircuits and associative memory. *Neural Netw.* **2009**, *22*, 1120–1128.
- [30] Reijmers, L. G.; Perkins, B. L.; Matsuo, N.; Mayford, M. Localization of a stable neural correlate of associative memory. *Science* **2007**, *317*, 1230–1233.
- [31] Hampp, N.; Thoma, R.; Zeisel, D.; Bröchle, C.; Oesterhelt, D. Bacteriorhodopsin variants for holographic pattern recognition. *Adv. Chem.* **1994**, *240*, 511–526.
- [32] Paek, E. G.; Jung, E. C. Simplified holographic associative memory using enhanced nonlinear processing with a thermoplastic plate. *Opt. Lett.* **1991**, *16*, 1034–1036.
- [33] Paek, E. G.; Psaltis, D. Optical associative memory using Fourier transform holograms. *Opt. Eng.* **1987**, *26*, 265428.
- [34] Abu-Mostafa, Y. S.; Psaltis, D. Optical neural computers. *Sci. Am.* **1987**, *256*, 88–95.
- [35] Popp, A.; Wolperdinger, M.; Hampp, N.; Bröchle, C.; Oesterhelt, D. Photochemical conversion of the O-intermediate to 9-cis-retinal-containing products in bacteriorhodopsin films. *Biophys. J.* **1993**, *65*, 1449–1459.
- [36] Gillespie, N. B.; Wise, K. J.; Ren, L.; Stuart, J. A.; Marcy, D. L.; Hillebrecht, J.; Li, Q.; Ramos, L.; Jordan, K.; Fyvie, S. et al. Characterization of the

- branched-photocycle intermediates P and Q of bacteriorhodopsin. *J. Phys. Chem. B* **2002**, *106*, 13352–13361.
- [37] Ranaghan, M. J.; Greco, J. A.; Wagner, N. L.; Grewal, R.; Rangarajan, R.; Koscielceki, J. F.; Wise, K. J.; Birge, R. R. Photochromic bacteriorhodopsin mutant with high holographic efficiency and enhanced stability via a putative self-repair mechanism. *ACS Appl. Mater. Interfaces* **2014**, *6*, 2799–2808.
- [38] Wagner, N. L.; Greco, J. A.; Ranaghan, M. J.; Birge, R. R. Directed evolution of bacteriorhodopsin for applications in bioelectronics. *J. R. Soc. Interface* **2013**, *10*, 20130197.
- [39] Hillebrecht, J. R.; Wise, K. J.; Koscielceki, J. F.; Birge, R. R. Directed evolution of bacteriorhodopsin for device applications. *Methods Enzymol.* **2004**, *388*, 333–347.
- [40] Dabbousi, B. O.; Rodriguez-Viejo, J.; Mikulec, F. V.; Heine, J. R.; Mattoussi, H.; Ober, R.; Jensen, K. F.; Bawendi, M. G. (CdSe)ZnS core-shell quantum dots: Synthesis and characterization of a size series of highly luminescent nanocrystallites. *J. Phys. Chem. B* **1997**, *101*, 9463–9475.
- [41] Alivisatos, A. P.; Gu, W. W.; Larabell, C. Quantum dots as cellular probes. *Annu. Rev. Biomed. Eng.* **2005**, *7*, 55–76.
- [42] Bruchez, M., Jr.; Moronne, M.; Gin, P.; Weiss, S.; Alivisatos, A. P. Semiconductor nanocrystals as fluorescent biological labels. *Science* **1998**, *281*, 2013–2016.
- [43] Carey, G. H.; Abdelhady, A. L.; Ning, Z. J.; Thon, S. M.; Bakr, O. M.; Sargent, E. H. Colloidal quantum dot solar cells. *Chem. Rev.* **2015**, *115*, 12732–12763.
- [44] Griep, M. H.; Winder, E. M.; Lueking, D. R.; Garrett, G. A.; Karna, S. P.; Friedrich, C. R. Förster resonance energy transfer between core/shell quantum dots and bacteriorhodopsin. *Mol. Biol. Int.* **2012**, *2012*, 910707.
- [45] Rakovich, A.; Nabiev, I.; Sukhanova, A.; Lesnyak, V.; Gaponik, N.; Rakovich, Y. P.; Donegan, J. F. Large enhancement of nonlinear optical response in a hybrid nanobiomaterial consisting of bacteriorhodopsin and cadmium telluride quantum dots. *ACS Nano* **2013**, *7*, 2154–2160.
- [46] Rakovich, A.; Sukhanova, A.; Bouchonville, N.; Lukashov, E.; Oleinikov, V.; Artemyev, M.; Lesnyak, V.; Gaponik, N.; Molinari, M.; Troyon, M. et al. Resonance energy transfer improves the biological function of bacteriorhodopsin within a hybrid material built from purple membranes and semiconductor quantum dots. *Nano Lett.* **2010**, *10*, 2640–2648.
- [47] Bouchonville, N.; Molinari, M.; Sukhanova, A.; Artemyev, M.; Oleinikov, V. A.; Troyon, M.; Nabiev, I. Charge-controlled assembling of bacteriorhodopsin and semiconductor quantum dots for fluorescence resonance energy transfer-based nanophotonic applications. *Appl. Phys. Lett.* **2011**, *98*, 013703.
- [48] Griep, M. H.; Walczak, K. A.; Winder, E. M.; Lueking, D. R.; Friedrich, C. R. Quantum dot enhancement of bacteriorhodopsin-based electrodes. *Biosens. Bioelectron.* **2010**, *25*, 1493–1497.
- [49] Roy, P.; Kantor-Uriel, N.; Mishra, D.; Dutta, S.; Friedman, N.; Sheves, M.; Naaman, R. Spin-controlled photoluminescence in hybrid nanoparticles purple membrane system. *ACS Nano* **2016**, *10*, 4525–4531.
- [50] Peck, R. F.; DasSarma, S.; Krebs, M. P. Homologous gene knockout in the archaeon *Halobacterium salinarum* with *ura3* as a counterselectable marker. *Mol. Microbiol.* **2000**, *35*, 667–676.
- [51] Becher, B. M.; Cassim, J. Y. Improved isolation procedures for the purple membrane of *Halobacterium halobium*. *Prep. Biochem.* **1975**, *5*, 161–178.
- [52] Nan, W. N.; Niu, Y.; Qin, H. Y.; Cui, F.; Yang, Y.; Lai, R. C.; Lin, W. Z.; Peng, X. G. Crystal structure control of zinc-blende CdSe/CdS core/shell nanocrystals: Synthesis and structure-dependent optical properties. *J. Am. Chem. Soc.* **2012**, *134*, 19685–19693.
- [53] Chen, O.; Zhao, J.; Chauhan, V. P.; Cui, J.; Wong, C.; Harris, D. K.; Wei, H.; Han, H.-S.; Fukumura, D.; Jain, R. K. et al. Compact high-quality CdSe/CdS core/shell nanocrystals with narrow emission linewidths and suppressed blinking. *Nat. Mater.* **2013**, *12*, 445–451.
- [54] Greenhalgh, D. A.; Altenbach, C.; Hubbell, W. L.; Khorana, H. G. Locations of Arg-82, Asp-85, and Asp-96 in helix C of bacteriorhodopsin relative to the aqueous boundaries. *Proc. Natl. Acad. Sci. USA* **1991**, *88*, 8626–8630.
- [55] Krebs, M. P.; Behrens, W.; Mollaaghababa, R.; Khorana, H. G.; Heyn, M. P. X-ray diffraction of a cysteine-containing bacteriorhodopsin mutant and its mercury derivative. Localization of an amino acid residue in the loop of an integral membrane protein. *Biochemistry* **1993**, *32*, 12830–12834.
- [56] Mollaaghababa, R.; Steinhoff, H.-J.; Hubbell, W. L.; Khorana, H. G. Time-resolved site-directed spin-labeling studies of bacteriorhodopsin. Loop-specific conformational changes in M. *Biochemistry* **2000**, *39*, 1120–1127.
- [57] Brizzolara, R. A.; Boyd, J. L.; Tate, A. E. Evidence for covalent attachment of purple membrane to a gold surface via genetic modification of bacteriorhodopsin. *J. Vac. Sci. Technol.* **1997**, *15*, 773–778.
- [58] Schranz, M.; Noll, F.; Hampp, N. Oriented purple membrane monolayers covalently attached to gold by multiple thiole linkages analyzed by single molecule force spectroscopy. *Langmuir* **2007**, *23*, 11134–11138.
- [59] Patil, A. V.; Premaruban, T.; Berthoumieu, O.; Watts, A.; Davis, J. J. Enhanced photocurrent in engineered bacteriorhodopsin monolayer films. *J. Phys. Chem. B* **2012**, *116*, 683–689.
- [60] Eliash, T.; Weiner, L.; Ottolenghi, M.; Sheves, M. Specific binding sites for cations in bacteriorhodopsin. *Biophys. J.* **2001**, *81*, 1155–1162.
- [61] Renugopalakrishnan, V.; Barbiellini, B.; King, C.; Molinari, M.; Mochalov, K.; Sukhanova, A.; Nabiev, I.; Fojan, P.; Tuller, H. L.; Chin, M. et al. Engineering a robust photovoltaic device with quantum dots and bacteriorhodopsin. *J. Phys. Chem. C* **2014**, *118*, 16710–16717.
- [62] Li, R.; Li, C. M.; Bao, H. F.; Bao, Q. Stationary current generated from photocycle of a hybrid bacteriorhodopsin/quantum dot bionanosystem. *Appl. Phys. Lett.* **2007**, *91*, 223901.
- [63] Yen, C.-W.; Chu, L.-K.; El-Sayed, M. A. Plasmonic field enhancement of the bacteriorhodopsin photocurrent during its proton pump photocycle. *J. Am. Chem. Soc.* **2010**, *132*, 7250–7251.
- [64] Uruga, T.; Hamaoka, T.; Kito, Y.; Uchida, I.; Nishimura, S.; Mashimo, T. Effects of volatile anesthetics on bacteriorhodopsin in purple membrane, *Halobacterium halobium* cells and reconstituted vesicles. *Biophys. Chem.* **1991**, *41*, 157–168.
- [65] Pandey, P. C.; Upadhyay, B. C.; Pandey, C. M. D.; Pathak, H. C. Dependence of M, N and O states decay kinetics of D96N bacteriorhodopsin on amine and amino compounds and its application in chemical sensing. *Sens. Actuators B* **1998**, *46*, 80–86.
- [66] Avi-Dor, Y.; Rott, R.; Schnaiderman, R. The effect of antibiotics on the photocycle and protoncycle of purple membrane suspensions. *Biochim. Biophys. Acta* **1979**, *545*, 15–23.
- [67] Chizhov, I.; Engelhard, M.; Chernavskii, D. S.; Zubov, B.; Hess, B. Temperature and pH sensitivity of the O<sub>640</sub> intermediate of the bacteriorhodopsin photocycle. *Biophys. J.* **1992**, *61*, 1001–1006.
- [68] Váró, G.; Lanyi, J. K. Protonation and deprotonation of the M, N, and O intermediates during the bacteriorhodopsin photocycle. *Biochemistry* **1990**, *29*, 6858–6865.
- [69] Kono, M.; Misra, S.; Ebrey, T. G. pH dependence of light-induced proton release by bacteriorhodopsin. *FEBS Lett.* **1993**, *331*, 31–34.
- [70] Greco, J. A.; N. L. Wagner, N. L.; Birge, R. R. Fourier transform holographic associative processors based on bacteriorhodopsin. *Int. J. Unconv. Comput.* **2012**, *8*, 433–457.
- [71] Oesterhelt, D.; Bräuchle, C.; Hampp, N. Bacteriorhodopsin: A biological material for information processing. *Quart. Rev. Biophys.* **1991**, *24*, 425–478.
- [72] Krivenkov, V. A.; Solovyeva, D. O.; Samokhvalov, P. S.; Brazhnik, K. I.; Kotkovskiy, G. E.; Christyakov, A. A.; Lukashev, E. P.; Nabiev, I. R. Photoinduced modification of quantum dot optical properties affects bacteriorhodopsin photocycle in a (quantum dot)-bacteriorhodopsin hybrid material. *J. Phys.: Conf. Ser.* **2014**, *541*, 012045.
- [73] Zaitsev, S. Y.; Lukashev, E. P.; Solovyeva, D. O.; Chistyakov, A. A.; Oleinikov, V. A. Controlled influence of quantum dots on purple membranes at interfaces. *Colloids Surf. B* **2014**, *117*, 248–251.
- [74] Bunkin, F. V.; Vsevolodov, N. N.; Druzko, A. B.; Mitsner, B. I.; Prokhorov, A. M.; Savranskii, V. V.; Tkachenko, N. W.; Shevchenko, T. B. Diffraction efficiency of bacteriorhodopsin and its analogs. *Sov. Tech. Phys. Lett.* **1981**, *7*, 630–631.
- [75] Vsevolodov, N. N.; Poldratskii, V. A. Holograms in biochrome, a biological photochromic material. *Sov. Phys. Tech. Phys.* **1985**, *30*, 1235–1247.
- [76] Korenstein, R.; Hess, B. Hydration effects on the photocycle of bacteriorhodopsin in the thin layers of purple membrane. *Nature* **1977**, *270*, 184–186.
- [77] Druzko, A. B.; Chamorovsky, S. K. The cycle of photochromic reactions of a bacteriorhodopsin analog with 4-keto-retinal. *BioSystems* **1995**, *35*, 133–136.
- [78] Beischel, C. J.; Mani, V.; Govindjee, R.; Ebrey, T. G.; Knapp, D. R.; Crouch, R. K. Ring oxidized retinals form unusual bacteriorhodopsin analogue pigments. *Photochem. Photobiol.* **1991**, *54*, 977–983.
- [79] Zeisel, D.; Hampp, N. Spectral relationship of light-induced refractive index and absorption changes in bacteriorhodopsin films containing wildtype BR<sub>w</sub> and the variant BRD<sub>96N</sub>. *J. Phys. Chem.* **1992**, *96*, 7788–7792.
- [80] Thorgeirsson, T. E.; Milder, S. J.; Miercke, L. J. W.; Betlach, M. C.; Shand, R. F.; Stroud, R. M.; Kliger, D. S. Effects of Asp-96 → Asn, Asp-85 → Asn, and Arg-82 → Gln single state substitutions on the photocycle of bacteriorhodopsin. *Biochemistry* **1991**, *30*, 9133–9142.

- [81] Cao, Y.; Brown, L. S.; Needleman, R.; Lanyi, J. K. Relationship of proton uptake on the cytoplasmic surface and reisomerization of the retinal in the bacteriorhodopsin photocycle: An attempt to understand the complex kinetics of the pH changes and the N and O intermediates. *Biochemistry* **1993**, *32*, 10239–10248.
- [82] Song, Q. W.; Zhang, C. P.; Gross, R.; Birge, R. Optical limiting by chemically enhanced bacteriorhodopsin films. *Opt. Lett.* **1993**, *18*, 775–777.
- [83] Schobert, B.; Cupp-Vickery, J.; Hornak, V.; Smith, S. O.; Lanyi, J. K. Crystallographic structure of the K intermediate of bacteriorhodopsin: Conservation of free energy after photoisomerization of the retinal. *J. Mol. Biol.* **2002**, *321*, 715–726.
- [84] Chu, L.-K.; Yen, C.-W.; El-Sayed, M. A. On the mechanism of the plasmonic field enhancement of the solar-to-electric energy conversion by the other photosynthetic system in nature (bacteriorhodopsin): Kinetic and spectroscopic study. *J. Phys. Chem. C* **2010**, *114*, 15358–15363.
- [85] Biesso, A.; Qian, W.; Huang, X. H.; El-Sayed, M. A. Gold nanoparticles surface plasmon field effects on the proton pump process of the bacteriorhodopsin photosynthesis. *J. Am. Chem. Soc.* **2009**, *131*, 2442–2443.
- [86] Rakovich, A.; Donegan, J. F.; Oleinikov, V.; Molinari, M.; Sukhanova, A.; Nabiev, I.; Rakovich, Y. P. Linear and nonlinear optical effects induced by energy transfer from semiconductor nanoparticles to photosynthetic biological systems. *J. Photochem. Photobiol. C* **2014**, *20*, 17–32.
- [87] Griep, M.; Mallick, G.; Lueking, D. R.; Friedrich, C. R.; Karna, S. P. Integration of optical protein and quantum dot films for biosensing. In *Proceedings of the 8<sup>th</sup> IEEE Conference on Nanotechnology*, Arlington, Texas, USA, 2008, pp 657–659.
- [88] Lee, T.-Y.; Yeh, V.; Chuang, J. L.; Chung Chan, J. C.; Chu, L.-K.; Yu, T.-Y. Tuning the photocycle kinetics of bacteriorhodopsin in lipid nanodiscs. *Biophys. J.* **2015**, *109*, 1899–1906.
- [89] Drachev, A. L.; Drachev, L. A.; Kaulen, A. D.; Khitrina, L. V. The action of lanthanum ions and formaldehyde on the proton-pumping function of bacteriorhodopsin. *Eur. J. Biochem.* **1984**, *138*, 349–356.
- [90] Hildebrandt, N.; Spillmann, C. M.; Algar, W. R.; Pons, T.; Stewart, M. H.; Oh, E.; Susumu, K.; Diaz, S. A.; Delehanty, J. B.; Medintz, I. L. Energy transfer with semiconductor quantum dot bioconjugates: A versatile platform for biosensing, energy harvesting, and other developing applications. *Chem. Rev.* **2017**, *117*, 536–711.
- [91] Stewart, M. H.; Huston, A. L.; Scott, A. M.; Oh, E.; Algar, W. R.; Deschamps, J. R.; Susumu, K.; Jain, V.; Prasuhn, D. E.; Blanco-Canosa, J. et al. Competition between Förster resonance energy transfer and electron transfer in stoichiometrically assembled semiconductor quantum dot-fullerene conjugates. *ACS Nano* **2013**, *7*, 9489–9505.
- [92] Allam, N. K.; Yen, C.-W.; Near, R. D.; El-Sayed, M. A. Bacteriorhodopsin/TiO<sub>2</sub> nanotube arrays hybrid system for enhanced photoelectrochemical water splitting. *Energy Environ. Sci.* **2011**, *4*, 2909–2914.